Supporting Information (SI)

Reconstructing Atomic Fe Coordination in PMS Activation Process to Realize Efficient BPA Degradation at Low Temperature

Yuxuan Lin,[#a] Weihua Qin,[#a] Yuwei Lu[a], Mingye Ren[a], Pan Gao[b], Feng Xiao[a] and Shaoxia Yang*[a]

[a] School of Water Resources and Hydropower Engineering, North China Electric Power University, Beijing, 102206, PR China

[b] School of Renewable Energy, North China Electric Power University, Beijing, 102206, PR China

[#] Author Contributions: Yuxuan Lin and Weihua Qin contributed equally.

***** Corresponding author: Shaoxia Yang (yangshaoxia2012@126.com)

Tel.: +86-10-61772456; Fax: +86-10-61772230.

The supplementary materials include 32 Pages, 2 Texts, 5 Tables, 17 Figures.

Contents

= 0.2 g/L, $[Catalyst]_0$ = 0.1 g/L, pH_0 = 6.8).

Fig. S8. TOC removal during BPA degradation in the Fe SACs/PMS systems ($[BPA]_0$ = 20 mg/L, PMS = 0.2 g/L, $[Catalyst]_0$ = 0.1 g/L, pH_0 = 6.8, T = 4°C).

Fig. S9. Comparison of the TOF over the reported nanocatalysts for the BPA degradation.

Fig. S10. The BPA removal.in the presence of inorganic anions in the Fenton-like reaction over the Fe–N/$P_{1.6}$–C SAC ($[BPA]_0$ = 20 mg/L, PMS = 0.2 g/L, $[Catalyst]_0$ = 0.1 g/L, pH_0 = 6.8, T = 4°C).

Fig. S11. The relationship between the initial reaction rates removing different pollutants over the Fe–N/$P_{1.6}$–C SAC and their IP values ($[BPA]_0$ = 20 mg/L, PMS = 0.2 g/L, $[Catalyst]_0$ = 0.1 g/L, pH_0 = 6.8, T = 4°C).

Fig. S12. Stability of the Fe–N/$P_{1.6}$–C SAC in the Fenton-like reaction for the BPA degradation ($[BPA]_0$ = 20 mg/L, PMS = 0.2 g/L, $[Catalyst]_0$ = 0.1 g/L, pH_0 = 6.8, T = 4°C).

Fig. S13. BPA removal over Fe-based catalysts alone with the addition of different (a) N or (b) P sources ($[BPA]_0$ = 20 mg/L, PMS = 0.2 g/L, $[Catalyst]_0$ = 0.1 g/L, pH_0 = 6.8, T = 4°C).

Fig. S14. EIS curves of the Fe–N/P_n–C SACs.

Fig. S15. Effect of SCN^- on BPA degradation in the Fe SACs/PMS system ($[BPA]_0$ = 20 mg/L, PMS = 0.2 g/L, $[Catalyst]_0$ = 0.1 g/L, $[SCN^-]_0$ = 4.38 mM, pH_0 = 6.8, T = 4°C).

Fig. S16. The simplified models of (a) Fe–N–C and (b) Fe–N/$P_{1.6}$–C SACs.

Fig. S17. PDOS of Fe–N–C and Fe–N/$P_{1.6}$–C SACs.

Text S1. Materials synthesis.

Synthesis of N/P–C catalyst. Similar to the synthesis of Fe–N/$P_{1.6}$–C SAC, 400 μL (6 mmol) of pyrrole monomer and 737 μL (0.8 mmol) of phytic acid were mixed with 2 mL of ethanol/water (v/v = 1:1). 684 mg (3 mmol) of ammonium persulfate was dissolved into another 6 mL of ethanol/water (v/v = 1:1). The subsequent steps were identical to those for Fe–N/$P_{1.6}$–C SAC to prepare N, P co-doped porous carbon materials, and the resulting samples were named as N/P–C catalyst.

Synthesis of N–C catalyst. Except for the addition of phytic acid, nitrogen-doped porous carbon (NC) was prepared by the same procedure as for N/P–C catalyst. The resulting sample was named as N–C catalyst.

Synthesis of Fe–N–C SAC. For the synthesis of Fe–N–C SAC, 10 mg of $FeCl_3 \cdot 6H_2O$ and 30 mg of 1,10-phenanthroline were added to 2 mL of ethanol, mixed well and added dropwise into 100 mg of N–C. The solution was stirred continuously at room temperature until it evaporated. Then, the powder was dried at 80 °C. After drying, the powder was calcinated at 700 °C for 2 h under an N_2 atmosphere at a heating rate of 5 °C/min. The final product was etched with 1 M H_2SO_4 at 80 °C for 2 h to produce Fe–N–C SAC.

Synthesis of Fe–P–C catalyst. Instead of standing overnight, the samples were aged at 70 °C for 2 h under stirring, and then dried at 80 °C overnight, except for the addition of pyrrole monomer. Then, only P-doped porous carbon materials were prepared by the same procedure as Fe–N/$P_{1.6}$–C SAC. The obtained sample was named as Fe–P–C catalyst.

Synthesis of Fe–N/P_n–C SACs. Consistent with the preparation of Fe–N/$P_{1.6}$–C SAC, the only difference was that phytic acids (0.2, 0.5, 1, and 1.5 mmol) were added to obtain catalysts with different N/P ratios (0.4, 1, 2, and 3).

Text S2. Contributions of diverse ROS to BPA oxidation in Fe–N/P_n–C/PMS systems.

On the basis of the BPA degradation in the presence of radical scavengers, the contributions of diverse ROS to BPA removal in Fe–N/P_n–C/PMS systems were determined as follows[1]:

$$\lambda(\bullet\,OH\&SO_4^{\bullet-}) = [(1 - C/C_0)_{Control} - (1 - C/C_0)_{TBA} - (1 - C/C_0)_{methanol}] \times 100\% \quad (S1)$$

$$\lambda(HO_2^{\bullet}/O_2^{\bullet-}) = [(1 - C/C_0)_{Control} - (1 - C/C_0)_{p\text{-}BQ}] \times 100\% \quad (S2)$$

$$\lambda(\,^1O_2) = 1 - \lambda(\bullet\,OH) - \lambda(HO_2^{\bullet}/O_2^{\bullet-}) \quad (S3)$$

Where $[1-(C/C_0)_{Control}]$ stands for the degradation efficiency of BPA in the absence of quenching agent, and $[1-(C/C_0)_{TBA}]$, $[1-(C/C_0)_{methanol}]$ and $[1-(C/C_0)_{p\text{-}BQ}]$ are the degradation efficiency of BPA after adding TBA, methanol, and p-BQ, respectively.

Table S1. High performance liquid chromatography (HPLC) operating conditions for organic analysis.

Compounds	Wavelength (nm)	Flow rate (mL/min)	Ultrapure water (%)	0.2% Acetic acid (%)	Acetonitrile (%)	Methanol (%)	Structural formula
BPA	276		30	-	-	70	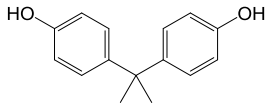
Phenol	254		-	40	-	60	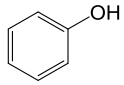
IBP	222		25	-	75	-	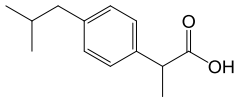
PHT	225	1.0	40	-	60	-	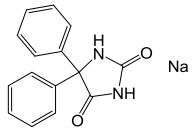
4-CP	280		40			60	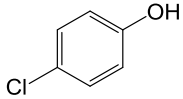
2,4-D	284			75		26	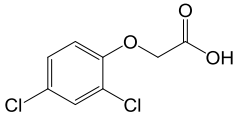

Table S2. Summary of Fe loading in the Fe–N–C SACs for activating PMS systems.

Catalyst	Loading (wt.%)	Reference
Fe–N/$P_{1.6}$–C	2.32	**This work**
Fe-N/C	0.88	2
SA-Fe/CN	0.62	3
SAFe-OCN	0.84	4
Fe–N–C	0.82	5
Fe-SAC	0.71	6
SA-Fe-NC	1.12	7
Fe-SAC	2.60	8

Table S3. Comparison of the BPA degradation over different SACs in the Fenton-like reaction for activating PMS near neutral pH.

Catalyst	BPA (mg/L)	Catalyst dosage (g/L)	PMS concentration (g/L)	T (°C)	Removal efficiency	TOF (L/(min·g))	E_a (kJ/mol)	Reference
Fe–N/$P_{1.6}$–C	20	0.2	0.2	25	98.3% (5 min)	24.49	3.7	**This work**
Co–N_2	20	0.2	0.2	30	100% (5 min)	3.47	-	1
Co–N_4–C	20	0.1	0.2	25	100% (60 min)	4.52	-	9
3SACu@NBC	20	0.1	0.4	25	100% (30 min)	1.57	-	10
Fe_{SA}–N–C–20	20	0.15	0.4	-	100% (20 min)	1.6	-	2
Mn–ISA@CN	20	0.2	0.2	25	100% (6 min)	5.69	-	11
NiZn@N–G–900	20	0.2	0.2	30	100% (80 min)	2.67	15.75	12
Cu–N_4/C–B	20	0.1	0.2	25	98% (5 min)	5.6	-	
Cu–N_4/C–P	20	0.1	0.2	25	11% (5 min)	0.08	-	13
Cu–N_4/C	20	0.1	0.2	25	57% (5 min)	1.02	-	

Table S4. Comparison on the BPA degradation over different Fe-based nanocatalysts in the Fenton-like reaction.

Catalyst	BPA (mg/L)	Catalyst dosage (g/L)	Oxidant	Oxidant concentration (mM)	pH	T (°C)	Removal efficiency	TOF (L/(min·g))	E_a (kJ/mol)	Reference
Fe–N/$P_{1.6}$–C	20	0.1	PMS	0.65	6.8	4	98.3% (5 min)	24.5	3.7	**This work**
GS–Fe–NPs	25	0.3	H_2O_2	1000	6.9	30	95% (140 min)	0.1067	128.8	14
MIL–101(Fe)	50	0.2	H_2O_2	10	6.0	30	100% (30 min)	1.75	46	15
$Fe_{0.8}Co_{2.2}O_4$	20	0.1	PMS	0.65	3.0	30	95% (60 min)	0.49	19.45	16
FeCA–g-C_3N_4	20	0.5	H_2O_2	10	4.0	-	92.5% (30 min)	0.17	-	17
Fe^{3+}@g-C_3N_4	20	0.2	PMS	0.65	3.0	-	100% (15 min)	3.02	-	18
Ag/AgCl/Fh	30	1	H_2O_2	5	3.0	-	100% (60 min)	0.05	-	19
CN–Cu(II)–$CuAlO_2$	25	1	H_2O_2	5	6-7	35	98% (120 min)	0.03	-	20
Fe–Co–85	20	0.2	H_2O_2	80	6.0	25	85% (6 min)	0.38	-	21

Table S5. Parameters of the obtained water samples.

	Secondary effluent	South-to-North Water Diversion
pH	6.56	8.36
TOC (mg/L)	5.22	3.07
Cl^- (mg/L)	6.05	0.23
HCO_3^- (mg/L)	21.36	-
SO_4^{2-} (mg/L)	47.62	23.49

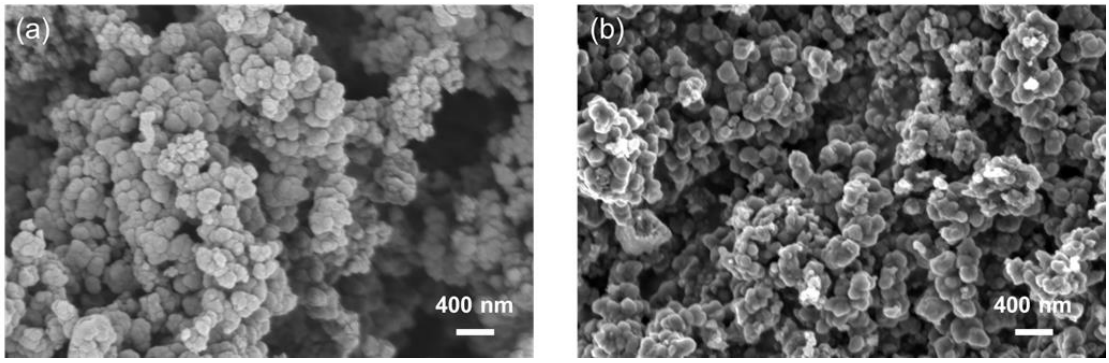

Fig. S1. SEM images of (a) Fe–N–C and (b) Fe–N/$P_{1.6}$–C SACs.

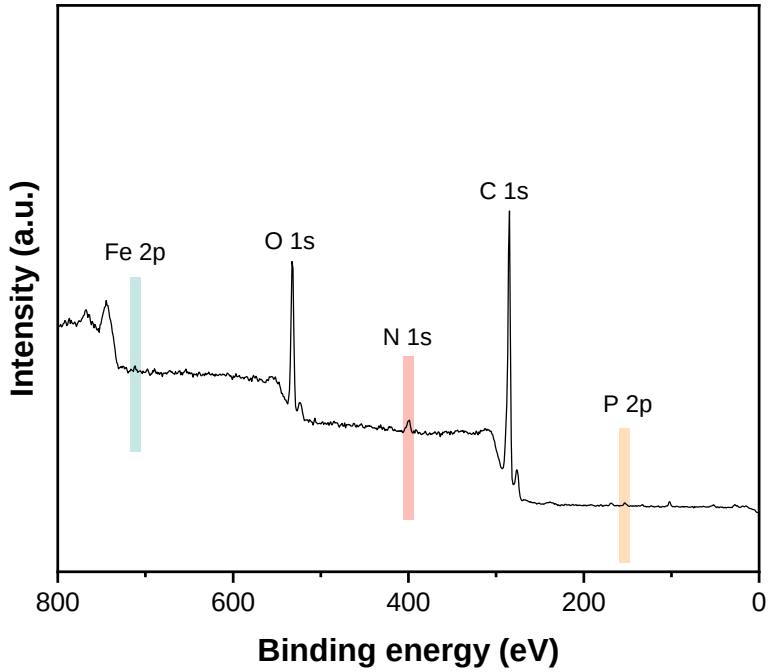

Fig. S2. XPS survey spectrum for the Fe–N/$P_{1.6}$–C SAC.

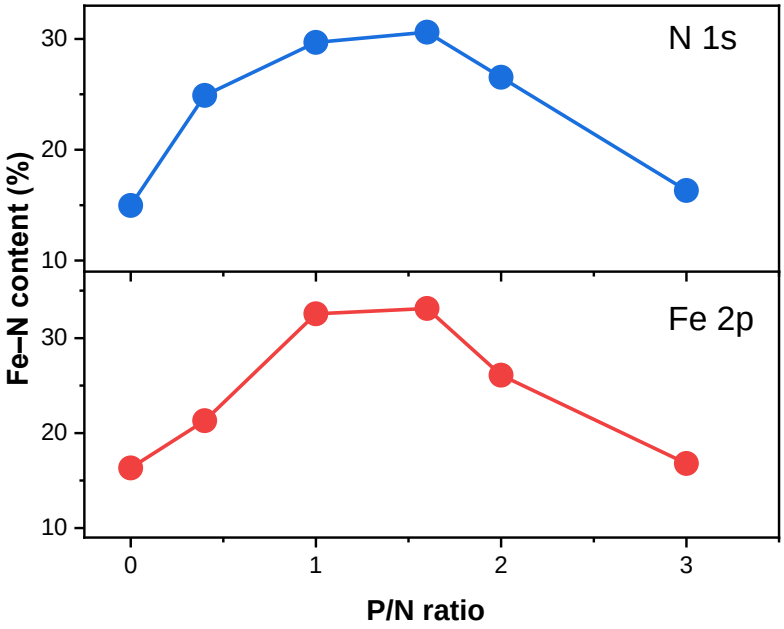

Fig. S3. Fe–N contents of N 1s and Fe 2p XPS spectra for the Fe–N/P_n–C SACs.

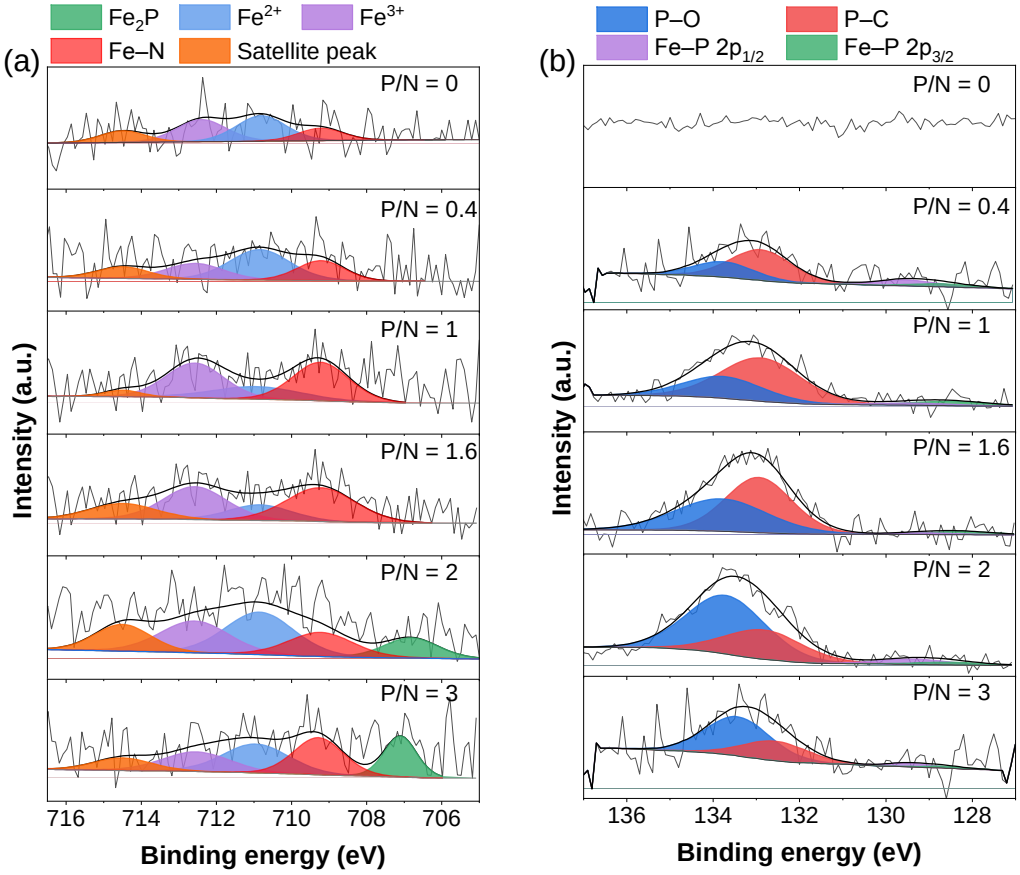

Fig. S4. XPS spectra of (a) Fe 2p and (b) P 2p for the Fe–N/P_n–C SACs.

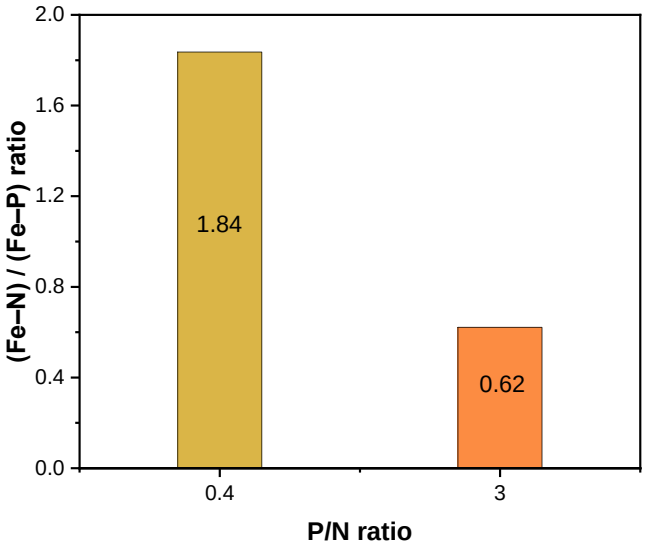

Fig. S5. The ratio of (Fe–N)/(Fe–P) for the Fe–N/P_n–C SACs.

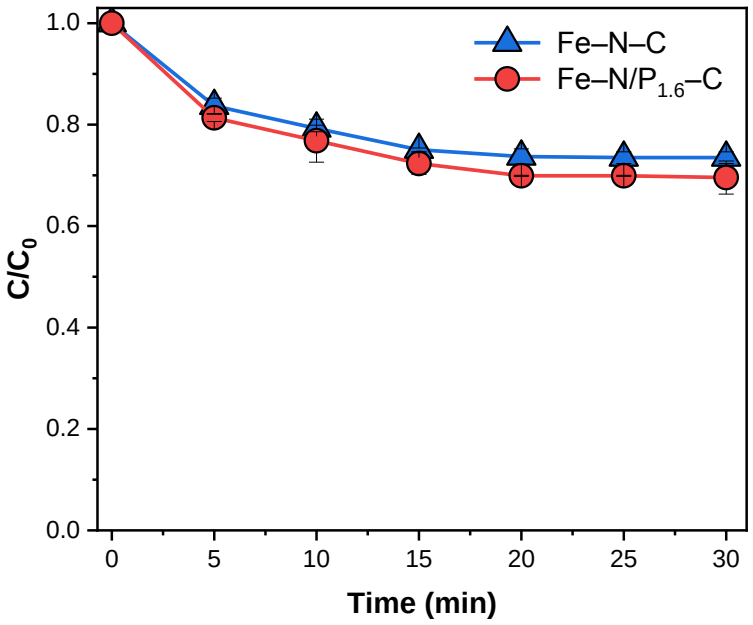

Fig. S6. Adsorption of BPA on the Fe SACs in the heterogeneous Fenton-like reaction ($[BPA]_0$ = 20 mg/L, $[Catalyst]_0$ = 0.1 g/L, pH_0 = 6.8, T = 4°C).

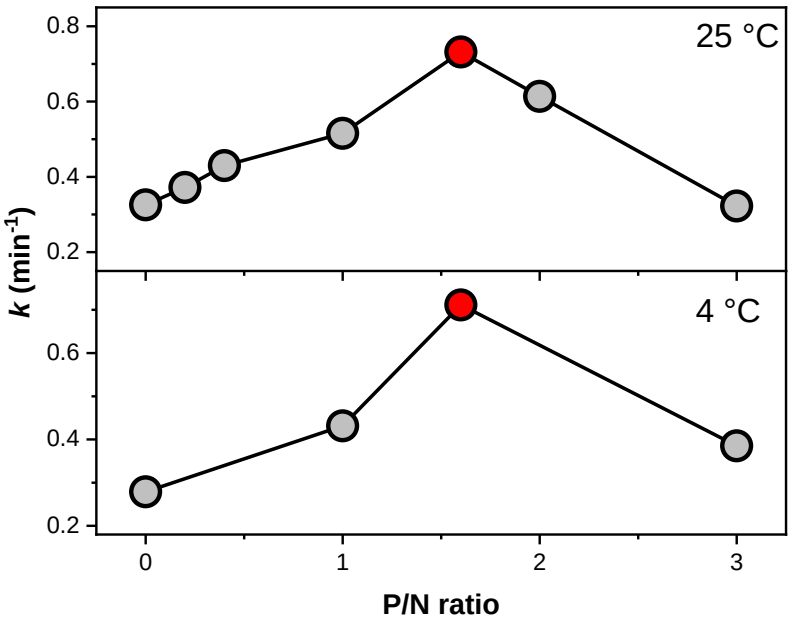

Fig. S7. Relationship between different P/N ratios of the Fe–N/P_n–C SACs and the initial reaction rate for the BPA degradation ($[BPA]_0$ = 20 mg/L, PMS = 0.2 g/L, $[Catalyst]_0$ = 0.1 g/L, pH_0 = 6.8).

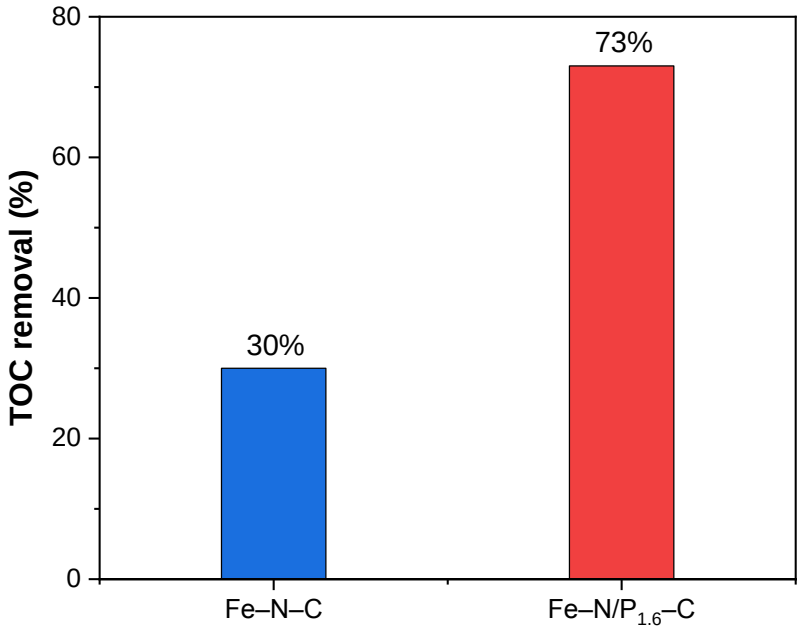

Fig. S8. TOC removal during BPA degradation in the Fe SACs/PMS systems ($[BPA]_0$ = 20 mg/L, PMS = 0.2 g/L, $[Catalyst]_0$ = 0.1 g/L, pH_0 = 6.8, T = 4°C).

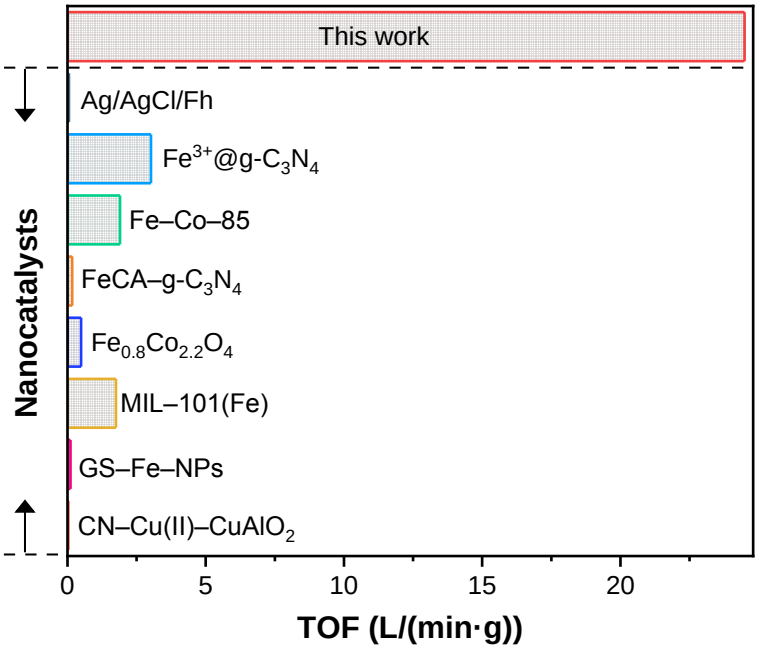

Fig. S9. Comparison of the TOF over the reported nanocatalysts for the BPA degradation.

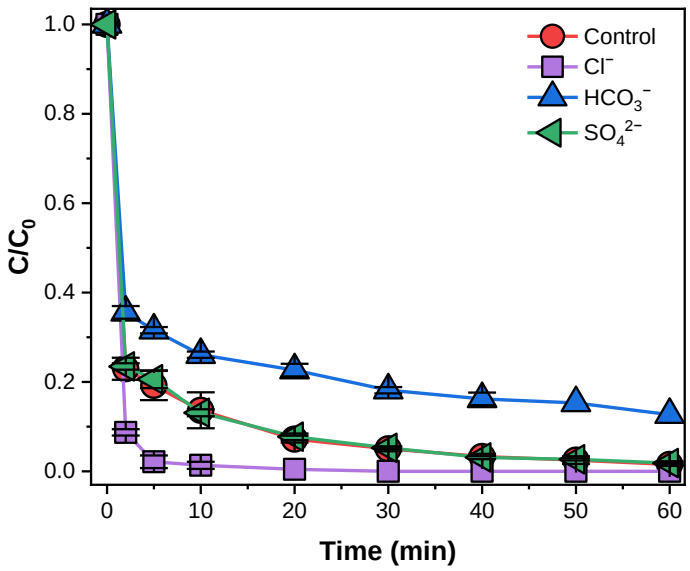

Fig. S10. The BPA removal in the presence of inorganic anions (Cl^-, HCO_3^-, SO_4^{2-}) in the Fenton-like reaction over the Fe–N/$P_{1.6}$–C SAC ($[BPA]_0$ = 20 mg/L, PMS = 0.2 g/L, $[Catalyst]_0$ = 0.1 g/L, pH_0 = 6.8, T = 4°C).

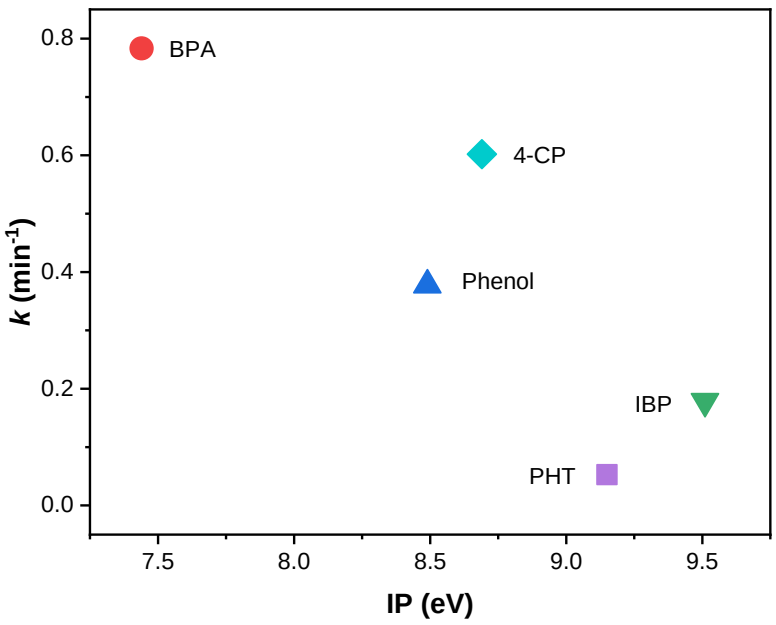

Fig. S11. The relationship between the initial reaction rates removing different pollutants over the Fe–N/$P_{1.6}$–C SAC and their IP values ($[BPA]_0$ = 20 mg/L, PMS = 0.2 g/L, $[Catalyst]_0$ = 0.1 g/L, pH_0 = 6.8, T = 4°C).

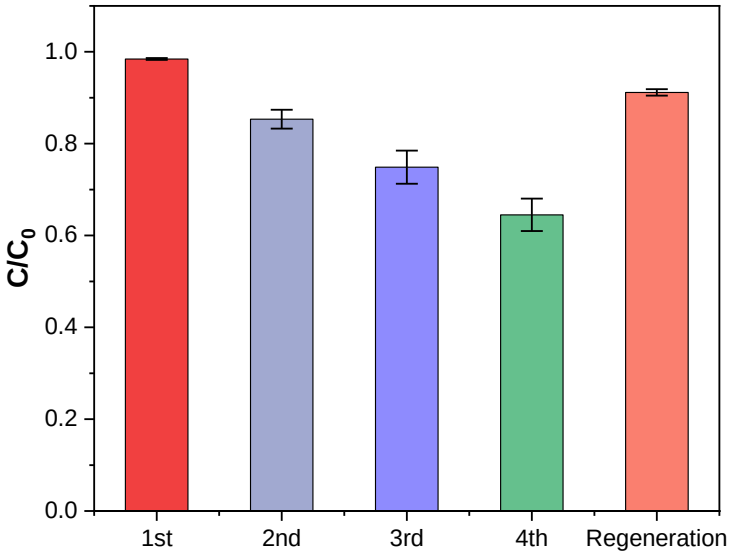

Fig. S12. Stability of the Fe–N/$P_{1.6}$–C SAC in the Fenton-like reaction for the BPA degradation ($[BPA]_0$ = 20 mg/L, PMS = 0.2 g/L, $[Catalyst]_0$ = 0.1 g/L, pH_0 = 6.8, T = 4°C).

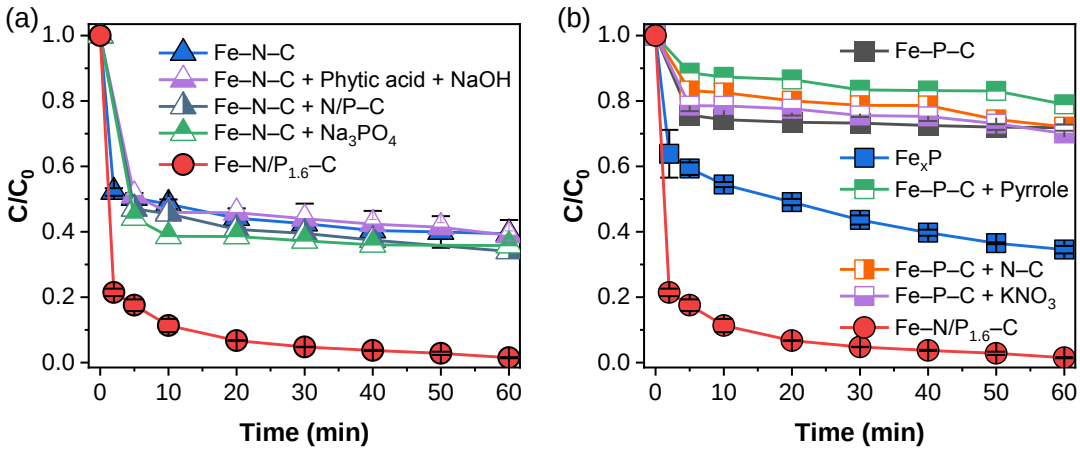

Fig. S13. BPA removal over Fe-based catalysts alone with the addition of different (a) N or (b) P sources ($[BPA]_0$ = 20 mg/L, PMS = 0.2 g/L, $[Catalyst]_0$ = 0.1 g/L, pH_0 = 6.8, T = 4°C).

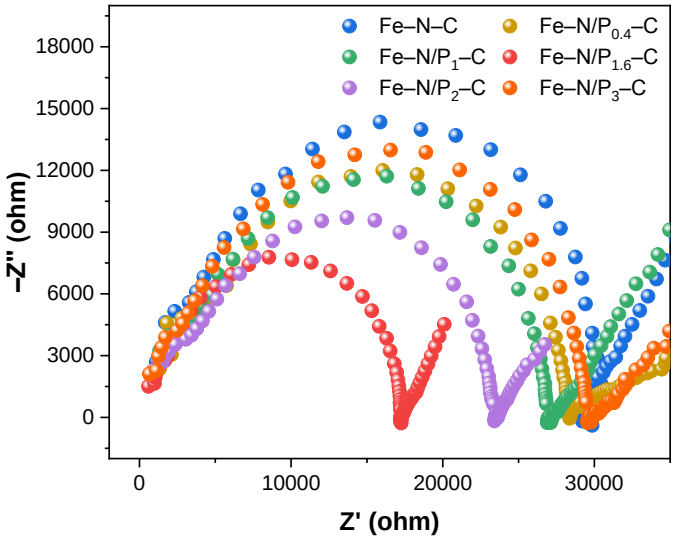

Fig. S14. EIS curves of the Fe–N/P_n–C SACs.

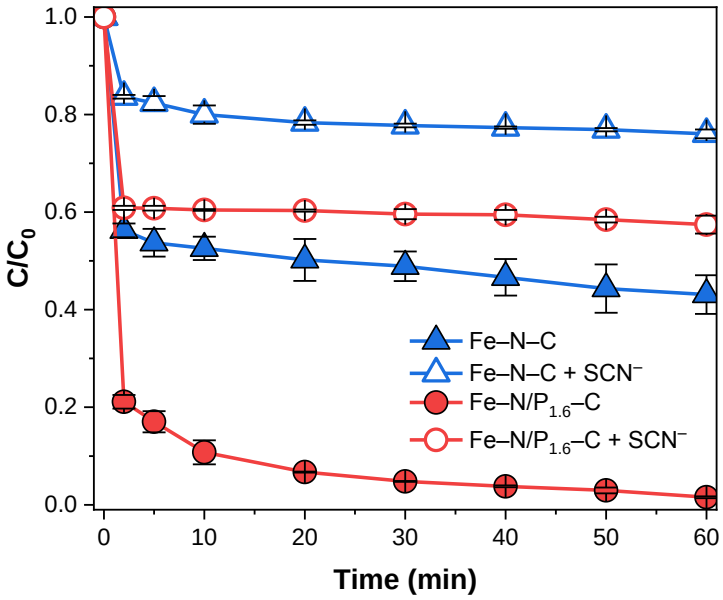

Fig. S15. Effect of SCN^- on BPA degradation in the Fe SACs/PMS system ($[BPA]_0$ = 20 mg/L, PMS = 0.2 g/L, $[Catalyst]_0$ = 0.1 g/L, $[SCN^-]_0$ = 4.38 mM, pH_0 = 6.8, T = 4°C).

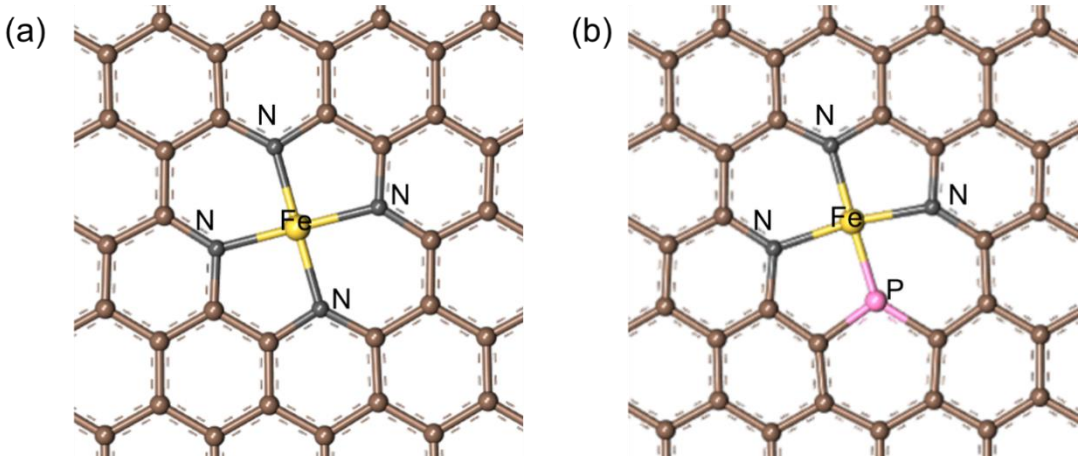

Fig. S16. The simplified models of (a) Fe–N–C and (b) Fe–N/$P_{1.6}$–C SACs.

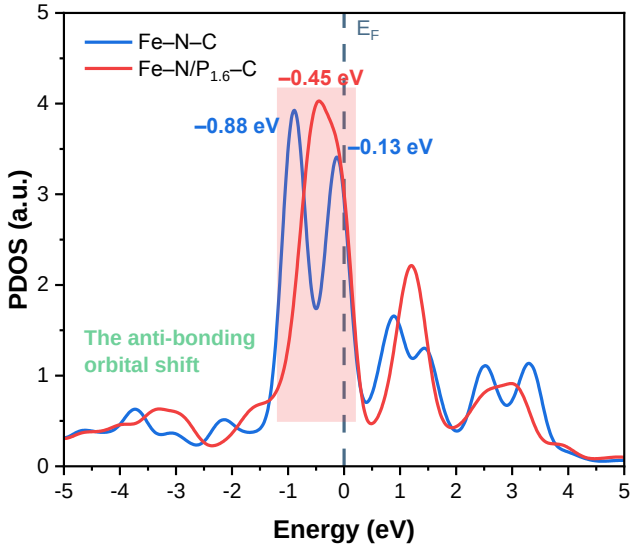

Fig. S17. PDOS of Fe–N–C and Fe–N/$P_{1.6}$–C SACs.

Reference

1. X. Liang, D. Wang, Z. Zhao, T. Li, Y. Gao and C. Hu, Coordination number dependent catalytic activity of single-atom cobalt catalysts for Fenton-like reaction, *Adv. Funct. Mater.*, 2022, **32**, 2203001.
2. T. Yang, S. Fan, Y. Li and Q. Zhou, Fe-N/C single-atom catalysts with high density of Fe-N_x sites toward peroxymonosulfate activation for high-efficient oxidation of bisphenol A: Electron-transfer mechanism, *Chem. Eng. J.*, 2021, **419**, 129590.
3. Y. Xiong, H. C. Li, C. W. Liu, L. R. Zheng, C. Liu, J. O. Wang, S. J. Liu, Y. H. Han, L. Gu, J. S. Qian and D. S. Wang, Single-atom Fe catalysts for Fenton-like reactions: Roles of different N species, *Adv. Mater*., 2022, **34**, 2110653.
4. Z. Zhou, M. Q. Li, C. G. Kuai, Y. X. Zhang, V. F. Smith, F. Lin, A. Aiello, D. P. Durkin, H. N. Chen and D. M. Shuai, Fe-based single-atom catalysis for oxidizing contaminants of emerging concern by activating peroxides, *J. Hazard. Mater*., 2021, **418**, 126294.
5. L. Peng, X. G. Duan, Y. N. Shang, B. Y. Gao and X. Xu, Engineered carbon supported single iron atom sites and iron clusters from Fe-rich Enteromorpha for Fenton-like reactions via nonradical pathways, *Appl. Catal. B-Environ*., 2021, **287**, 119963.
6. Y. Gao, T. W. Wu, C. D. Yang, C. Ma, Z. Y. Zhao, Z. H. Wu, S. J. Cao, W. Geng, Y. Wang, Y. Y. Yao, Y. N. Zhang and C. Cheng, Activity trends and mechanisms in peroxymonosulfate-assisted catalytic production of singlet oxygen over atomic

metal-N-C catalysts, *Angew. Chem. Int. Edit*., 2021, **60**, 22513-22521.

7. Y. W. Gao, Y. Zhu, T. Li, Z. H. Chen, Q. K. Jiang, Z. Y. Zhao, X. Y. Liang and C. Hu, Unraveling the high-activity origin of single-atom iron catalysts for organic pollutant oxidation via peroxymonosulfate activation, *Environ. Sci. Technol*., 2021, **55**, 8318-8328.
8. M. Yang, R. Wu, S. Cao, Y. Li, S. Huo, W. Wang, Z. Hu and X. Xu, Versatile pathways for oxidating organics via peroxymonosulfate activation by different single atom catalysts confining with Fe–N_4 or Cu–N_4 sites, *Chem. Eng. J*., 2023, **451**, 138606.
9. M. Yang, Z. Hou, X. Zhang, B. Gao, Y. Li, Y. Shang, Q. Yue, X. Duan and X. Xu, Unveiling the origins of selective oxidation in single-atom catalysis via Co–N_4–C intensified radical and nonradical pathways, *Environ. Sci. Technol.*, 2022, **56**, 11635–11645.
10. J. Pan, B. Gao, P. Duan, K. Guo, M. Akram, X. Xu, Q. Yue and Y. Gao, Improving peroxymonosulfate activation by copper ion-saturated adsorbent-based single atom catalysts for the degradation of organic contaminants: electron-transfer mechanism and the key role of Cu single atoms, *J. Mater. Chem. A*, 2021, **9**, 11604-11613.
11. J. Yang, D. Zeng, Q. Zhang, R. Cui, M. Hassan, L. Dong, J. Li and Y. He, Single Mn atom anchored on N-doped porous carbon as highly efficient Fenton-like catalyst for the degradation of organic contaminants, *Appl. Catal. B-Environ.*, 2020, **279**, 119363.

12. J. J. You, C. Y. Zhang, Z. L. Wu, Z. M. Ao, W. Y. Sun, Z. K. Xiong, S. J. Su, G. Yao and B. Lai, N-doped graphite encapsulated metal nanoparticles catalyst for removal of Bisphenol A via activation of peroxymonosulfate: A singlet oxygen-dominated oxidation process, *Chem. Eng. J.*, 2021, **415**, 128890.

13. X. Zhou, M.-K. Ke, G.-X. Huang, C. Chen, W. Chen, K. Liang, Y. Qu, J. Yang, Y. Wang, F. Li, H.-Q. Yu and Y. Wu, Identification of Fenton-like active Cu sites by heteroatom modulation of electronic density, *Proc. Natl. Acad. Sci. U. S. A.*, 2022, **119**, e2119492119.

14. B. Guo, T. T. Xu, L. Zhang and S. Li, A heterogeneous Fenton-like system with green iron nanoparticles for the removal of bisphenol A: Performance, kinetics and transformation mechanism, *J. Environ. Manage.*, 2020, **272**, 111047.

15. P. P. Huang, L. L. Yao, Q. Chang, Y. H. Sha, G. D. Jiang, S. H. Zhang and Z. Li, Room-temperature preparation of highly efficient NH_2-MIL-101(Fe) catalyst: The important role of -NH_2 in accelerating Fe(III)/Fe(II) cycling, *Chemosphere*, 2022, **291**, 133026.

16. X. Li, Z. H. Wang, B. Zhang, A. I. Rykov, M. A. Ahmed and J. H. Wang, $Fe_xCo_{3-x}O_4$ nanocages derived from nanoscale metal-organic frameworks for removal of bisphenol A by activation of peroxymonosulfate, *Appl. Catal. B-Environ.*, 2016, **181**, 788-799.

17. Y. Yin, R. X. Jia, W. M. Zhang, Y. Ren, X. Y. Li, M. Hua and L. Lv, Electron-rich oxygen enhanced Fe-doped g-C_3N_4 mediated Fenton-like process: Accelerate Fe(III) reduction and strengthen catalyst stability, *J. Clean. Prod.*, 2021, **319**,

128680.

18. H. C. Li, C. Shan and B. C. Pan, Fe(III)-doped g-C_3N_4 mediated peroxymonosulfate activation for selective degradation of phenolic compounds via high-valent iron-oxo species, *Environ. Sci. Technol*., 2018, **52**, 2197-2205.

19. Y. P. Zhu, R. L. Zhu, Y. F. Xi, T. Y. Xu, L. X. Yan, J. X. Zhu, G. Q. Zhu and H. P. He, Heterogeneous photo-Fenton degradation of bisphenol A over Ag/AgCl/ferrihydrite catalysts under visible light, *Chem. Eng. J.*, 2018, **346**, 567-577.

20. L. Lyu, D. B. Yan, G. F. Yu, W. R. Cao and C. Hu, Efficient destruction of pollutants in water by a dual-reaction center Fenton-like process over carbon nitride compounds-complexed Cu(II)-$CuAlO_2$, *Environ. Sci. Technol.*, 2018, **52**, 4294-4304.

21. J. Y. Liu, X. N. Li, B. Liu, C. X. Zhao, Z. C. Kuang, R. S. Hu, B. Liu, Z. M. Ao and J. H. Wang, Shape-controlled synthesis of metal-organic frameworks with adjustable Fenton-like catalytic activity, *ACS Appl. Mater. Interfaces*., 2018, **10**, 38051-38056.